The quantitative analysis of the bilayer thickness and internal density fluctuation is possible, while the maximum diameter of the vesicle (ca. 240 nm) by far exceeds the maximum resolution of our SAXS experiments. The theoretical descriptions of scattering functions from a multilamellar stack of bilayers can be summarized as follows.[57] Assuming monodisperse bilayers, the scattered intensity $I(q)$ can be written as the product of the form factor $P(q)$ of the bilayers and the structure factor $S(q)$ describing their spatial arrangement similarly to that of globular particle systems:

$$I(q) \propto P(q)S(q) \quad (6)$$

When the thickness of the bilayer is sufficiently smaller than the lengthscale of the remaining two other dimensions as well as the radius of curvature of the bilayer, the form factor $P(q)$ in eq.(6) can be replaced with the product of the so-called Lorentz factor, $1/q^2$, and the thickness form factor or scattering function, $P_t(q)$.[58]

$$P(q) = (2\pi A/q^2)P_t(q) \quad (7)$$

where A is the area of the basal plane. Substituting $P_t(q)$ for $P(q)$, $I(q)$ in eq.(6) can be rewritten in the convenient form

$$I(q) \propto P_t(q)S(q)/q^2 \quad (8)$$

The thickness scattering function $P_t(q)$ is the cosine transformation of the thickness distance distribution function (thickness PDDF) $p_t(r)$. Therefore, we can use a similar method to a conventional indirect Fourier transformation (IFT)[59] to deduce $p_t(r)$ from the experimental $P_t(q)$.[58]

$$P_t(q) = 2\int_0^\infty p_t(r)\cos(qr)\mathrm{d}r \quad (9)$$

In the case of the absence of interlamellar interference peaks and their signature (no bilayer stacking as to be expected for vesicle solutions), we can assume $S(q) = 1$ in eq.(6). Figure 2c presents the calculated thickness PDDF, $p_t(r)$, of the vesicle designed for Hb encapsulation. We have already shown that the surface modification with low density poly(ethyleneglycol) (PEG) is quite efficient for long-term storage of the HbV, inhibiting intervesicular aggregation and fusion.[48, 60] However, due to the low density of PEG for surface modification of the vesicle as the concentration of DSPE-PEG is as low as 0.3 mol% of the total lipids, we were not able to observe the effect of PEG in $p_t(r)$. Nevertheless, $p_t(r)$ deduced without using any geometrical model reveals the thickness of the bilayer excluding PEG layer to be ca. 5.8 nm, which is read out from the distance (r-value) where $p_t(r)$ goes to zero, as highlighted in Figure 2c. Recently, we studied static structure and molecular dynamics in PEG-lipid (DSPE-PEG) micellar solutions with different molecular weights of PEG, M_{PEG}, by means of SAXS and dielectric relaxation spectroscopy (DRS).[61] The thickness of the hydrated PEG layer was estimated to be 8-9 nm for $M_{PEG} = 5000$. Due to different density and configuration, the extension of polymer chains in solution

may not necessarily be identical in the micelle and on the surface of the vesicle, it is apparent that the actual total bilayer thickness involving the surface PEG layer must be far greater than 5.8 nm.

The positive-negative-positive behavior of $p_t(r)$ when going from $r = 0$ to higher-r values is directly connected to the occurrence of positive and negative internal electron density layers within the bilayer. Theoretically, $p_t(r)$ is given by the convolution square of the electron density profile $\Delta\rho(r)$ perpendicular to the midplane of the bilayers, which is given by

$$p_t(r) = 2\int_0^\infty \Delta\rho(r')\Delta\rho(r'+r)\mathrm{d}r' \quad (10)$$

To extract more intuitive pictures of the internal structure of the bilayer, we performed a deconvolution procedure of the experimental $p_t(r)$ into $\Delta\rho(r)$ using a convolution square-root technique.[62-64] In Figure 2d, we display $\Delta\rho(r)$ obtained from the deconvolution analysis of $p_t(r)$ shown in Figure 2c. The innermost (the smallest-r) negative density part apparently reflects hydrophobic chain of the lipids. The following plateau having nearly zero electron density fluctuation, or an identical electron density with that of solvent water including salt, indicates localized cholesterol molecules on the hydrophobic/hydrophilic interface.[65] A terminal hydroxyl group is expected to be oriented toward the hydrophilic site of the lipids. The positive density layer seen in $1.7 \leq r/\mathrm{nm} \leq 2.9$ is attributed to the hydrophilic headgroup of the lipids. We note that the forward SAXS intensity is generally very sensitive not only to the structure but also the temperature dependent contrast. The pronounced difference in the forward intensities and different positions of the minimum in $I(q)$ at different temperatures as shown in Figure 2b sensitively reflect different contrast as a function of temperature. IFT and deconvolution analyses[62-64] given in Figures 2c and 2d demonstrate the stable bilayer structure, which does not significantly depend on temperature.

Hierarchical structures of HbV and the solution state of the encapsulated Hbs. The HbVs are hierarchically organized cellular-type artificial oxygen carrier that encapsulates a concentrated Hb solution in phospholipid vesicles, one HbV particle containing ca. 30000 Hb molecules. Figure 3 shows the SAXS intensity, $I(q)$, of the concentrated HbV dispersion ([Hb] = 10 g dL^{-1}, [solutes] = 16 g dL^{-1}; volume fraction, ca. 40%). We successfully measured more than five orders of magnitude of the scattered intensity (ca. 3.5×10^5 time-different maximum and minimum intensities), covering the extremely wide q-range of 0.06 - 10 nm^{-1}, which was quite essential for exploring the internal structures of HbV at the molecular level.

First, we checked the concentration dependence of $I(q)$ by diluting the dense stock HbV dispersion ([Hb] = 10 g dL^{-1}) with saline solution, and found virtually no concentration dependence of the shape of the scattering functions. This means that the effect of inter-particle interactions or static structure factor

$S(q)$, which is given as the Fourier transform of the total correlation function $[g(r)-1]$ and whose first peak position is expected to be $q = \sim 0.025$ nm^{-1} when hardsphere (HS) interaction and a 120nm radius are assumed, is not visible on the experimental $I(q)$ in our accessible q-range ($q > 0.06$ nm^{-1}). Consistent with the DLS results, the forward intensity of the HbV dispersion exhibits a typical feature of to some extent polydisperse spherical particles. In Figure 3, we added a theoretical scattering function calculated by accounting for the averaged diameter (~ 240 nm) and the size distribution obtained by DLS (green line, adjusted in height to the experimental intensity). Suppose that the HbV has homogeneous electron density distribution inside the particle, $I(q)$ should rapidly decrease proportional to q^{-4}, according to the theoretical curve for homogenous spheres. However, we clearly observed an enhanced excess scattering in the regime $2 \le q/\text{nm}^{-1} \le 10$. This high-$q$ excess component manifests the internal electron density fluctuations of the HbV particle, reflecting the shorter lengthscale structures of the encapsulated Hb solution and the lipid bilayer.

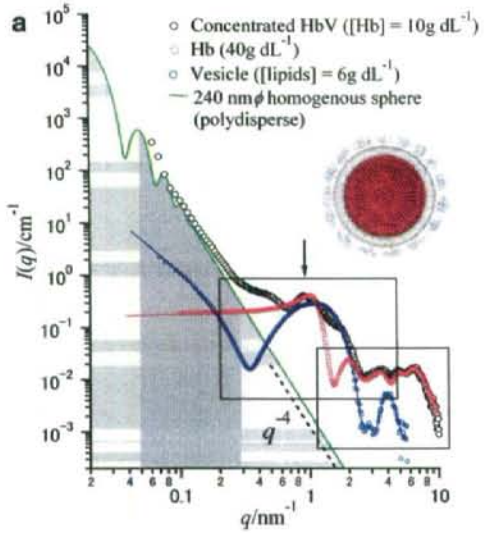

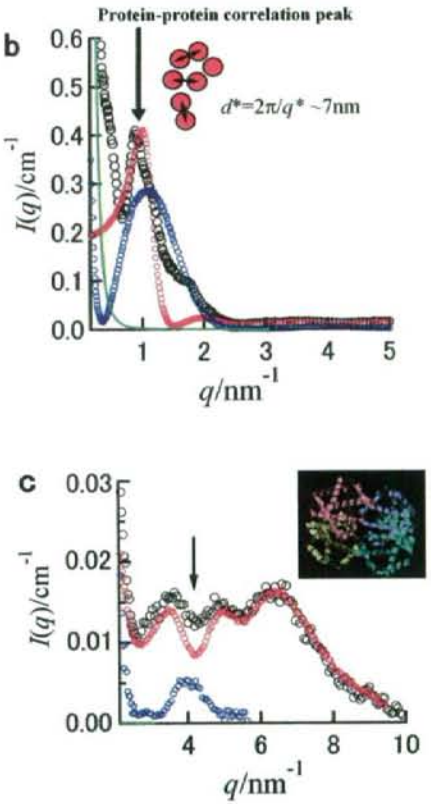

Figure 3: X-ray scattered intensity $I(q)$ in a log-log plot of the concentrated HbV dispersion ([Hb] = 10 g dL^{-1}) at 25 °C in $0.06 \le q/\text{nm}^{-1} \le 10$ is shown on absolute scale. A schematic picture of HbV is inserted into the panel **a** as well as a simulated scattering curve of a solution of polydisperse spheres according to the DLS results. In the panels **b** and **c**, the enlarged views of the high-q range are displayed in a lin-lin plot to visualize the significant features of $I(q)$ for protein-protein correlation peak and microscopic intramolecular structure of the encapsulated Hbs. Molecular structure of Hb is inserted in the panel **c**.

If we carefully look at the two specific q-ranges indicated by the two squares placed in Figure 3a, which are magnified in Figures 3b and 3c, we are able to access the information on the protein-protein interactions in the confined space of the aqueous phase of the HbV and the microscopic intra molecular structure of Hb molecules. As shown in Figures 3b and 3c, we found that the high-q part of $I(q)$ of the HbV is well approximated by a superposition of the experimental scattering functions of the concentrated Hb solution with identical concentration (ca. 38 g dL^{-1}) and of the phospholipids bilayer membrane (empty vesicles). Generally, for globular colloidal particle systems like proteins and micelles, the position, height, and width of the first peak of $S(q)$ strongly depends on the interparticle interactions determined e.g. by the radius, volume fraction, effective charge of the particles, a screening effect of electrostatic interaction, surface adhesion, and so forth.[53, 61, 66-69] The details of the concentration and temperature dependence of the Hb-Hb interactions in relation to the biological functions of Hb will be reported elsewhere. Importantly, we found that the protein-protein correlation peak position as well as the height and width of the first peak of $S(q)$ of the encapsulated Hbs are almost identical to those of a normal Hb solution with identical concentration (Figures 3b). The finding suggests that confinement effects into a ca. 240ϕ nm space are not very significant for the interparticle interaction potential of Hbs.

Figure 3c confirms the perfect coincidence of the scattering functions for the encapsulated and normal (bulk) Hbs in $2 \le q/\text{nm}^{-1} \le 10$, where the small difference between those of HbV and the normal Hb solution seen in $3 \le q/\text{nm}^{-1} \le 5$, highlighted by an arrow, can clearly be explained in terms of the contribution from the encapsulating vesicle. This implies unbiased intramolecular structures of Hb before and after its encapsulation into HbV.

Particle diffusion dynamics in a concentrated HbV dispersion. One of the most significant specificities of the HbV compared to any other conventional liposomal products is its extremely high concentration ([Hb] = 10 g dL^{-1}; [lipids] = 6 g dL^{-1}). This comes essentially from the requirement for achieving an oxygen-carrying capacity comparable to that of blood. As a result, the HbV dispersion for practical medical use is totally turbid due to high concentration and the sub-micron particle size. DLS techniques are often successfully used for observing diffusion processes of particle systems, thus being efficient for characterizing microscopic motion and inter particle interactions of particles. However, conventional DLS techniques that rely on a singly scattered signal are no longer applicable for such a dense, turbid system because of multiple scattering. In addition, absorption of hemoprotein is also a specific problem for the HbV system to be overcome. Therefore, we needed to efficiently reduce the scattering volume of the sample to observe microscopic motions of the HbV particles without diluting the samples. To overcome the obstacles, we used a modified thin-layer cell dynamic light-scattering (TC-DLS) technique.[42,43] As shown in the inset of Figure 4a, the concentrated HbV ([Hb] = 10 g dL^{-1})

dispersion inserted into the thin-layer cell (50 μm thick) is transparent as if it were a red cellophane sheet. The opposite side can be seen through the TC window, as 'HbV' written on a paper is readable without mistiness, and thus DLS experiments in the forward direction become possible. The total scattering angle in air was fixed to 41° for all the experiments, which corresponds to 29° in water, resulting in $q = 6.75 \times 10^{-3}$ nm^{-1}.

Figure 4 shows the concentration dependence of the normalized intensity correlation functions, $[g_2(\tau)\text{-}1]/\beta$, of the concentrated HbV dispersions measured at $q = 6.75 \times 10^{-3}$ nm^{-1}, which is lower than an anticipated HbV-HbV correlation peak position $q \sim 0.025$ nm^{-1} (See Figure 5). With increasing concentration from [Hb] = 1.0 g dL^{-1} to 5.0 g dL^{-1}, the short-time decay of $g_2(\tau)$ becomes faster, as excepted for the corrective diffusion of all repulsively interacting hardsphere (HS) systems. At the same time, we found the stretch of the long-time tail of $g_2(\tau)$, which may seem to indicate the occurrence of the gradual slowdown of the long-time behavior. With the further increase to [Hb] =10 g dL^{-1}, in turn, the short-time decay of $g_2(\tau)$ becomes slower, which is opposite to what is anticipated for a repulsively interacting system, and may imply the existence of weak attractive (adhesive) potential between HbVs. We may need to perform further experimental works to seek to understand the details of the interaction potentials between the HbVs. Nevertheless, the present TC-DLS data confirm that $g_2(\tau)$ for the most concentrated stock HbV dispersion ([Hb] =10 g dL^{-1}) rapidly converges to the baseline (unity) showing single-step behavior, which demonstrates, from a viewpoint of the particle diffusion dynamics, that the HbV dispersion is an ergodic system. The finding well supports good dispersion stability and proved long term preservation, owing to the applied surface modification of the HbV with poly(ethylene glycol) (PEG).

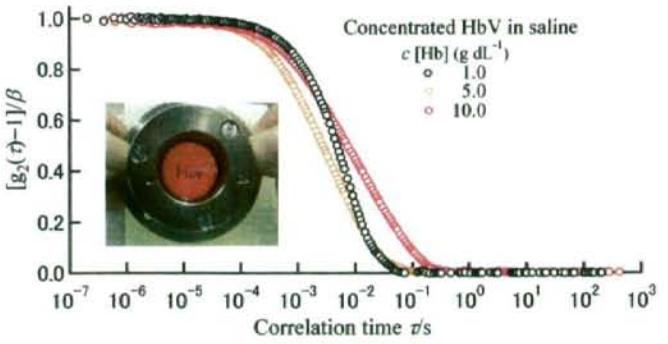

Figure 4: The normalized intensity correlation functions, $[g_2(\tau)-1]/\beta$, of the concentrated dispersions of the HbV at [Hb] = 1.0, 5.0, and 10 g dL^{-1}, as obtained by a modified thin-layer cell dynamic light-scattering (TC-DLS) technique at $q = 6.75 \times 10^{-3}$ nm^{-1}.

The effect of plasma substitutes on HbV-HbV interactions. Since the HbV does not contribute to colloid osmotic pressure (COP) of blood, upon anticipated actual medical treatments, the HbV must be dispersed with aqueous solution of plasma substitutes (water-soluble polymers) to adjust COP. Recently, Sakai et al. reported the rheological properties of the HbV dispersion ([Hb] = 10 g dL^{-1}) in a series of plasma substitute solutions with various molecular structures and molecular weights, such as recombinant human serum albumin (rHSA), dextran (DEX), modified fluid gelatin (MFG), and hydroxylethyl starch (HES).[32] They found that among these polymers, only HbV suspended in rHSA behaves nearly as a Newtonian fluid. In contrast, other plasma substitutes, such as HES, DEX, and MFG, induce non-Newtonian behavior of the HbV dispersions in particular for high molecular weight HES. Microchannel flow experiments indicated that this is due to flocculation of HbV in the presence of plasma substitutes. To gain insights into the mechanism of the HbV flocculation, we use different DLS techniques in this section.

Simulated static structure factors with depletion interaction potential. The depletion interaction potential[26-28] for hardsphere having the diameter σ in the presence of nonadsorbing polymers with the radius of gyration R_g can be approximated in the range of $\sigma < r < \sigma + 2R_g$ as[29]

$$u(r) = -\eta_p^{(R)} k_B T \frac{3}{2}\frac{1+\xi}{\xi^3}\left(\frac{r}{\sigma} - 1 - \xi\right)^2 \quad (11)$$

where r is the center-of-mass to center-of-mass distance between the two particles, $\xi = 2R_g/\sigma$ is the size ratio, corresponding to the dimensionless range of the depletion attraction, $\eta_p^{(R)}$ is the reservoir polymer volume fraction, which can be calculated from the volume fraction of the large particles ϕ and the size ratio ξ.[30] From Eq.11, one can easily find that the depth of the depletion potential is closely related to the two key parameters of ξ and $\eta_p^{(R)}$; the stronger attractive force between the two large particles is induced for smaller ξ and larger $\eta_p^{(R)}$. We simulated the pair correlation functions, $g(r)$, and the resulting static structure factors, $S(q)$, for the model systems of a very diluted HbV suspended in a series of plasma substitutes using depletion interaction potential model and SMSA closure relation.[70,71]

In Figure 5, we present $g(r)$ and $S(q)$ calculated assuming the diameter σ = 240 nm and volume fraction $\phi = 0.001$ to account for the HbV. To give ξ, the radius of gyration of the plasma substitutes determined by SAXS at c = 1.0 g dL^{-1} (unpublished results) was used; 5.5 nm (MFG), 4.96 nm (DEX), 2.84 nm (rHSA), 5.96 nm (HES$_{70}$), 6.83 nm (HES$_{130}$), and 12.95 nm (HES$_{670}$). The solution structures

of these plasma substitutes, involving the Flory radius, screening length, persistence length, and lengthscale-dependent fractal dimensions of the polymer chains will be reported elsewhere. We selected half of the original concentration of commercially available plasma substitutes; 2.5 g dL^{-1} (rHSA), 5.0 g dL^{-1} (DEX), 2.0 g dL^{-1} (MFG), 3.0 g dL^{-1} (HES$_{70}$), 3.0 g dL^{-1} (HES$_{130}$), and 3.0 g dL^{-1} (HES$_{670}$). In these calculations, we rely on the depletion potential and SMSA closure. According to the theoretical phase diagram,[30,31] the selected concentration of DEX seems to be already in the two phase region even at such a dilute concentration of the vesicle (to distinguish, $S(q)$ and $g(r)$ for DEX are given using a dashed line), while theoretically, others are still in one-phase fluid region.

In terms of the increased osmotic compressibility and coordination number manifested respectively in the $S(q)$ and $g(r)$, we estimated the effect of the different plasma substitutes on the flocculation tendency of the HbV particles to be in the order of DEX > MFG> HES$_{670}$ > HES$_{70}$ > HES$_{130}$ > rHSA. We will examine the validity of this prediction using DLS technique in the next sub-section.

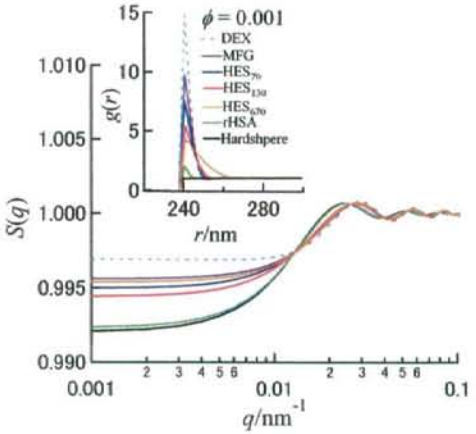

Figure 5: Simulated static structure factors $S(q)$ and pair correlation functions $g(r)$ of the model systems accounting for a dilute HbV suspended in the series of plasma substitutes. $g(r)$ and $S(q)$ were calculated using a depletion interaction potential for monodisperse hardspheres in the presence of nonadsorbing polymers and SMSA closure relation. We chose the diameter σ = 240 nm and volume fraction $\phi = 0.001$ to account for HbV in a dilute suspension, and the diameter $2R_g$ for small particles (polymers), where radius of gyration the plasma substitutes determined by SAXS at c = 1.0g dL^{-1} (unpublished results) was used for R_g. We assumed the situation that HbVs are suspended in plasma substitutes having half of the

original concentration, i.e. 2.5 g dL^{-1} (rHSA), 5.0 g dL^{-1} (DEX), 2.0 g dL^{-1} (MFG), 3.0 g dL^{-1} (HES_{70}), 3.0 g dL^{-1} (HES_{130}), and 3.0 g dL^{-1} (HES_{670}).

Effects of plasma substitutes on the HbV diffusion dynamics in a diluted dispersion. To start with the simplest case, we first tried to investigate variation of the particle diffusion dynamics of the vesicle (without Hb encapsulation) in a diluted suspension in the presence of plasma substitutes and its polymer-concentration dependence. Figure 6 shows the intensity correlation functions, $g_2(t)$, of a diluted vesicle ([lipids] = 0.012 g dL^{-1}) dispersed in various plasma substitute solutions of rHSA, DEX, MFG, HES_{70}, HES_{130}, and HES_{670}, measured at $q = 0.223$ nm^{-1}. The concentrations of these plasma substitutes are varied from 10% to 100% of their original concentrations, while fixing vesicle concentration. Figure 7a shows $g_2(t)$ of the vesicle/rHSA systems. With increasing rHSA concentration, two distinct decays become clearly visible. The faster decay is apparently attributed to the diffusion of rHSAs, and the slower one is to that of the vesicles. Importantly, we observed that $g_2(t)$ at different rHSA concentrations almost simultaneously converges to the baseline at about the same point, demonstrating that a significant slowdown of the vesicle diffusion is not induced by rHSA.

The appearance of two distinct decays is common for all polymers. However, in contrast to the case of rHSA, we found that, as can be seen from Figures 6b-e, all other plasma substitutes cause a pronounced slowdown of the vesicle translational diffusion, and the effect becomes significantly stronger with increasing polymer concentration. In Figure 7, we display the intensity distribution functions $D_I(R_H)$ of vesicle dispersions calculated using ORT[56] from the same DLS data shown in Figure 6a-f, where the data at highest plasma substitute concentrations were chosen. Figure 7 underlines that rHSA does not cause the vesicle flocculation, but other polymers do. In terms of $D_I(R_H)$, the efficacy of the plasma substitutes on the vesicle flocculation are estimated to be in the order of DEX > HES_{670} > MFG > HES_{130} > HES_{70} > rHSA, instead of DEX > MFG> HES_{670} > HES_{70} > HES_{130} > rHSA that is predicted from the depletion potential model. In light of the results, the tendency can broadly be explained with depletion interaction, but there exist some singularity of HES series; (i) the influence of HES_{670} is considerably stronger than expected and (ii) the effect of HES_{130} is stronger than that for HES_{70}, which is opposite to the theoretical prediction. These are likely to be due to unideality of the systems involving the distribution of molecular weights and the complexity of the polymer chain structure.

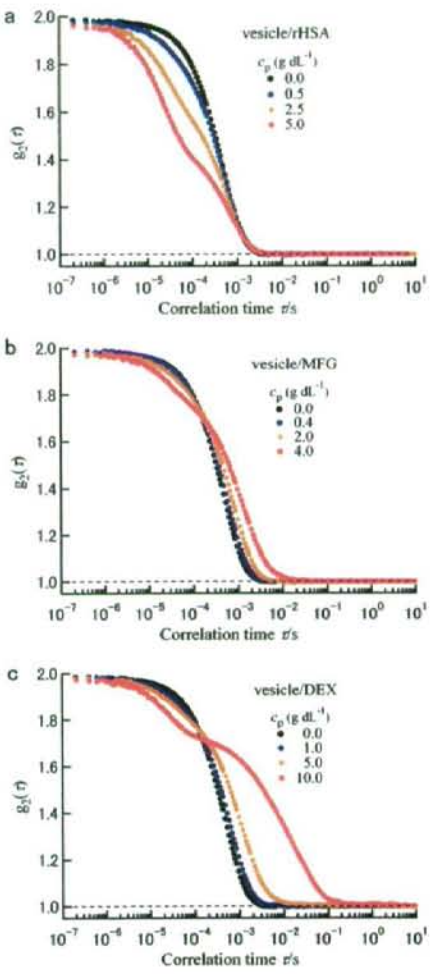

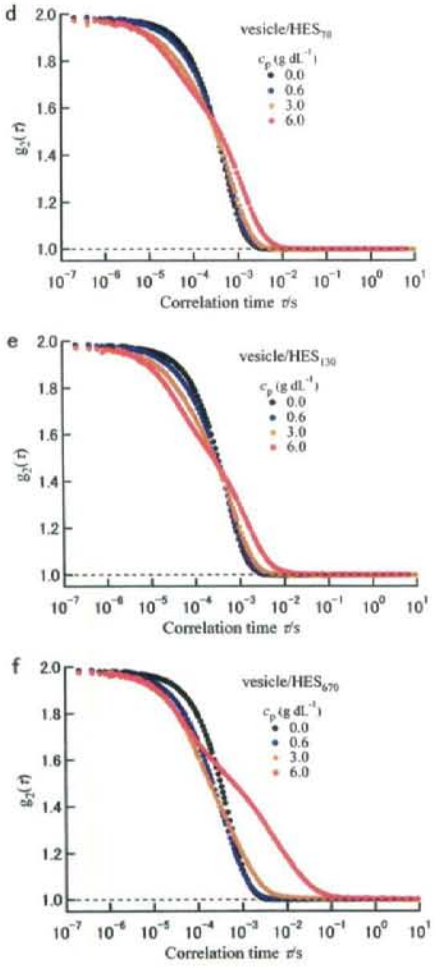

Figure 6: The intensity correlation functions, $g_2(t)$, of a 0.012 g dL^{-1} vesicle suspended in various plasma substitute solutions of rHSA, DEX, MFG, HES_{70}, HES_{130}, and HES_{670}, measured at q = 0.223 nm^{-1}. The concentrations of the plasma substitutes are adjusted to 10%, 50%, and 100% of their original concentration by dilution with saline solution.

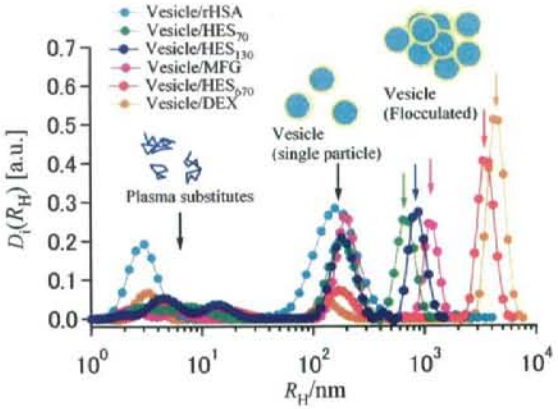

Figure 7: Effect of plasma substitutes on vesicle flocculation in a dilute suspension. The intensity distribution functions, $D_1(R_H)$, of a 0.012 g dL^{-1} vesicle suspended in various plasma substitute solutions of rHSA, DEX, MFG, HES_{70}, HES_{130}, and HES_{670} as a function of hydrodynamic radius, R_H. $D_1(R_H)$ was calculated form the intensity correlation functions, $g_2(t)$, presented in Figure 6 using ORT procedure.[56]

In Figure 8, a partial phase diagram of HbV/polymer mixtures as a function of ϕ_{HbV}, $\eta_p^{(R)}$, and ξ is presented together with a typical theoretical phase diagram of a colloid-polymer mixture (ξ = 0.08),[27] where the reservoir polymer volume fractions $\eta_p^{(R)}$ is estimated for different plasma substitutes at half of their original concentrations; 2.5 g dL^{-1} (rHSA), 5.0 g dL^{-1} (DEX), 2.0 g dL^{-1} (MFG), 3.0 g dL^{-1} (HES_{70}), 3.0 g dL^{-1} (HES_{130}), and 3.0 g dL^{-1} (HES_{670}), using the radius of gyration R_g determined with SAXS data at 1.0 g dL^{-1} (unpublished data). The filled and empty circles represent single liquid and two phases, respectively. In practice, other conditions, e.g., polydispersity and surface charge of the large particle as well as non-ideality of polymer structure especially at high $\eta_p^{(R)}$ may affect the phase behavior. Nevertheless, the figure imply that the phase separation of the HbV suspension in the presence of the

plasma substitutes can be understood based on the depletion interaction potential model for hardsphere mixed with non-adsorbing polymers.

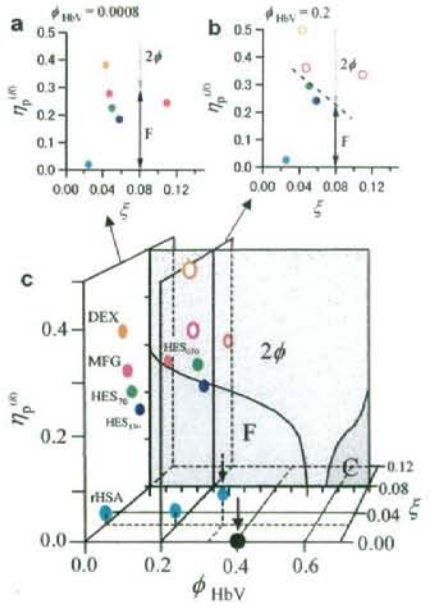

Figure 8: Partial phase diagram of HbV in the presence of plasma substitutes as a function of HbV volume fraction ϕ_{HbV}, reservoir polymer volume fractions $\eta_p^{(R)}$, and the polymer to HbV size ratio ξ, shown together with a theoretical phase diagram of a colloid-polymer mixture ($\xi = 0.08$).[27] Panels **a** and **b** represent 2-D phase diagrams at ϕ_{HbV} = 0.0008 and ϕ_{HbV} = 0.2, respectively, and **c** presents a 3-D diagram as a function of ϕ_{HbV}, $\eta_p^{(R)}$, and ξ. F, C, and 2ϕ on the theoretical phase diagram indicate single phase fluid, crystal, and two phase regions, respectively. For ϕ_{HbV} = 0.0008 and 0.2, the concentration of plasma substitutes was fixed to half of their original ones, i.e., 2.5 g dL^{-1} (rHSA: light blue), 5.0 g dL^{-1} (DEX: orange), 2.0 g dL^{-1} (MFG: pink), 3.0 g dL^{-1} (HES$_{70}$: right green), 3.0 g dL^{-1} (HES$_{130}$: blue), and 3.0 g dL^{-1} (HES$_{670}$: red). Filled and empty circles represent single phase fluid and two-phase, respectively. Arrows highlight the stock HbV dispersion (ϕ_{HbV} = 0.4) and a currently major applicatory HbV/rHSA mixture (ϕ_{HbV} = 0.32) used for preclinical tests.

The effects of plasma substitutes on the HbV diffusion dynamics in a dense dispersion. We used TC-DLS to study concentrated HbV/plasma substitute mixtures. In Figures 9a and 9b, we present $g_2(t)$ of the concentrated HbV ([Hb] = 5 g dL^{-1}, [lipids] = 3 g dL^{-1}) and the vesicle without Hb encapsulation ([lipids] = 3 g dL^{-1}) suspended in saline solution and in a series of different plasma substitute solutions of rHSA, HES$_{70}$, and HES$_{130}$. In the presence of these plasma substitutes, the decay of $g_2(t)$ becomes apparently slower, indicating the induced depletion forces by plasma substitute (Figures 9a). As shown in Figure 9b, we confirmed that with no reference to Hb-encapsulation, $g_2(t)$ exhibits a similar trend.

In Figure 9c, we compare the TC-DLS result on the concentrated HbV ([Hb] = 8 g dL^{-1}) suspended in 5 g dL^{-1} rHSA solution to that of the dense stock HbV dispersion ([Hb] = 10 g dL^{-1}) in saline solution. We note that rHSA is currently a leading candidate for the co-injected plasma substitute, and most pre-clinical tests of the HbV were carried out using rHSA.[8,9] These two samples exhibit similar single-step behavior of $g_2(t)$ and a rapid decrease to the baseline. This observation provides evidence for ergodicity of these two samples as a nature of single fluid phase, which supports the results obtained in the previous rheological study.

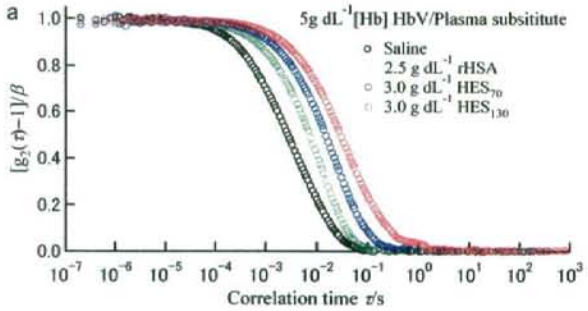

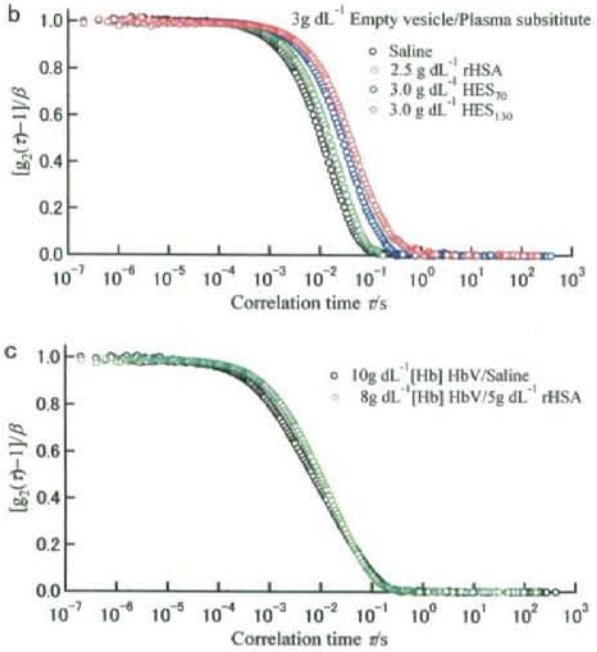

Figure 9: The intensity correlation functions, $g_2(\tau)$, of the concentrated dispersions of HbV and empty uni-lamellar vesicles in saline and plasma substitute solutions; $g_1(\tau)$ of the concentrated HbV dispersions at [Hb] = 1.0, 5.0, and 10 g dL^{-1} (a), the HbV ([Hb] = 5.0 g dL^{-1}) suspended in 2.5 g dL^{-1} rHSA, 3.0 g dL^{-1} HES$_{70}$, and 3.0 g dL^{-1} HES$_{130}$ solutions (b), the 3.0 g dL^{-1} vesicle in the same series of plasma substitutes (c), and the stock HbV dispersion ([Hb] = 10 g dL^{-1}) and the applicatory HbV ([Hb] = 8 g dL^{-1}) in a 5 g dL^{-1} rHSA dispersion in actual medical applications.

Effects of large-molecular-weight HES on the particle motions of HbV. If the HbV is suspended at [Hb] = 5 g dL^{-1} in high concentration solutions of HES$_{670}$, MFG, or DEX, the occurrence of HbV flocculation is apparent. HbV exhibits gradual sedimentation and phase separation, as a red blood cell (RBC) does in normal blood. Note that no hemolysis was observed in these flocculating systems. To

explore the arrested dynamics in the flocculating dispersion, we employed bruteforce[44] and echo DLS[43-45] experiments. The multi-speckle averaging can be achieved in the bruteforce technique by step-by-step altering the sample configurations and performing repeated short time measurements. For a long-time part of (τ> 10 s), the sample cell was precisely rotated to explore many independent sample geometries during one evolution of the rotation to observe echo peaks. The time averaging can essentially be identical with the ensemble averaging.

In Figure 10, we display the field correlation function, $g_1(\tau)$, of the concentrated HbV ([Hb] = 5 g dL^{-1}, [lipids] = 3 g dL^{-1}) dispersed in a series of 3 g dL^{-1} HES solutions. The data of HbV/HES$_{670}$ dispersion were measured with the brute-force and echo DLS techniques in the TC configuration, and other $g_1(\tau)$ functions for HbV in saline and in the lower-molecular-weight HES solutions (HES$_{130}$ and HES$_{70}$) are converted from the same $g_2(\tau)$ data already shown in Figure 9a. In contrast to the rapid single-step relaxation behavior and apparently ergodic nature of the HbV/saline, HbV/HES$_{70}$, and HbV/HES$_{130}$ systems, the HbV/HES$_{670}$ dispersion shows a significant slowdown of the particle diffusion dynamics and looks like nonergodic within our time window (up to 3 × 10^4 sec). The process is characterized by the two-step behavior of $g_1(t)$, showing a faster decay with a small amplitude of ca. 0.15, and the following second slower decay. This observation demonstrates that the short-range particle diffusion is highly restricted in a flocculating system due to the depletion (polymer-induced adhesive) interaction between the HbV particles. The slower decay appears to reflect the slow dynamics of the large HbV flocculation in a HbV rich-phase of the phase separated dispersion, which certainly involves an aging effect during the echo experiment. Although we did not perform echo measurements for the HbV/DEX and HbV/MFG dispersions, repeated short-time DLS measurements with rotating the sample cell gave strong fluctuations of the intercept (coherence factor). This is a clear signature of the non-ergodicity or gradual phase-separation of these samples.

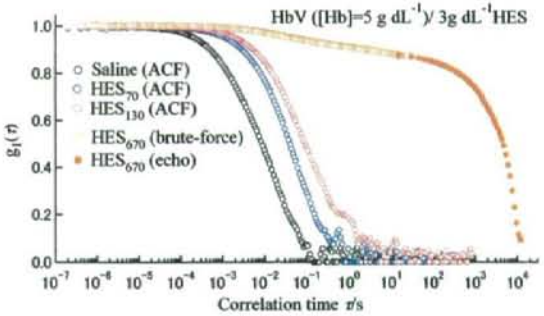

Figure 10: The field correlation functions, $g_1(t)$, of the concentrated HbV ([Hb] = 5 g dL^{-1}, [Lipids] = 3 g dL^{-1}) dispersed in saline and in a series of HES solutions. The $g_1(t)$ of the HbV/HES$_{670}$ was measured using bruteforce and echo DLS techniques in the thin layer cell configuration. The $g_1(t)$ data on the HbV in saline and in the lower-molecular-weight HES solutions (HES$_{70}$ and HES$_{130}$) were converted from the $g_2(t)$ data shown in Figure 9a.

Conclusions

We have investigated static structure and dynamics of HbV, a cellular-type artificial oxygen carrier functionalized as a transfusion alternative. DLS data on a diluted HbV dispersion evaluated by optimized regularization technique (ORT) yielded an averaged hydrodynamic diameter of 238 nm and a 20 nm standard deviation in volume distribution. The SAXS data on the vesicle for Hb encapsulation confirmed its uni-lamellar structure as designed, and the IFT analysis provided the thickness (ca. 5.8 nm) and internal electron density profiles of the bilayer membrane. Consistent with the DLS data, the forward SAXS intensity of the HbV dispersion exhibits a feature of polydisperse spherical particles having an averaged radius of ca 120 nm, while its high q-part manifests the internal density fluctuations reflecting the structure of the encapsulated Hb solution. We found that the position, height, and width of static structure factor of the encapsulated Hbs are quite similar to those in bulk Hb solution at identical protein concentration. The finding demonstrates that confinement into an inner aqueous phase of the vesicle (ca. 240 nm ϕ) does not significantly affect the interparticle interaction of Hbs. TC-DLS combined with the bruteforce and echo technique enables us to overcome the interference from multiple scattering of a turbid sample and thus makes it possible to observe collective diffusion of a concentrated HbV dispersion in the presence of various plasma substitutes (water-soluble polymers used to maintain colloid osmotic pressure of blood in medical treatments) without dilution. It should also be mentioned that this technique is perfectly non-invasive, i.e. no external force is applied to the system like in rheology. During the duration of these experiments, the HbV dispersions were perfectly stable. Actually, we confirmed that the dispersion stability of HbV and the oxygen binding function of encapsulated HbV were preserved for over two years at room temperature.[48] In contrast to the rapid single-step relaxation behavior and apparently ergodic nature of the HbV/saline, HbV/HES$_{70}$, and HbV/HES$_{130}$ systems, the HbV/HES$_{670}$ dispersion shows two-step behavior of $g_1(t)$, which looks like nonergodic within our time window; a faster decay with a small amplitude and the following second slower decay indicate that the short-range particle diffusion is strongly restricted in a flocculating system due to the depletion interaction between the HbV particles, while the slow mode appears to reflect the slow dynamics of the

HbV flocculation in a HbV rich-phase of the phase separated dispersion. We note that as we confirmed in the previous rheological study,[32] such a HbV flocculation dissociates rapidly under a shear flow and is completely reversible.

Despite a controversy on the mechanism of liposome flocculation, our DLS results, simulated structure factor, and the phase behavior, demonstrate that the underlying mechanism of the HbV flocculation in the presence of plasma substitutes is due to depletion interaction; exclusion of polymer molecules from the region closely spaced HbV particles induces an effective attractive potential between the HbVs, increasing the overall disorder of the system. At the same time, a pending question about a significantly weaker effect of rHSA on HbV flocculation and suspension viscosity enhancement than those induced by other polymers is clearly answered. This is attributed to a compact native structure of the protein, which efficiently reduces the reservoir polymer volume fraction, and thus suppresses the strength of the depletion forces. The significance of these entropically driven phenomena is highlighted by the tunable suspension rheology of HbVs using different combination of plasma substitute solutions. High viscosity fluid is occasionally advantageous for sustaining peripheral blood flow, giving shear stress on the vascular wall to facilitate the production of vasorelaxation factors. The results are not only implicative in the fields of soft-condensed matter physics and bio-chemistry, but of interdisciplinary importance for a new class of forthcoming medical applications.

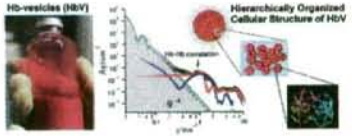

Acknowledgement The authors thank Dr. Dominique Erni (Inselspital Hospital, Univ. of Berne), Dr. Amy G. Tsai (Univ. of San Diego), Dr. Masahiko Takaori (East Takarazuka Sato Hospital), and Dr. Koichi Kobayashi (Keio Univ.) for their cooperation and meaningful discussions. This work was supported in part by Health Sciences Research Grants (Research on Publicly Essential Drugs and Medical Devices, H18-Soyaku-Ippan-022), from the Ministry of Health, Labour and Welfare, Japan (H.S., E.T.), Grants-in-Aid for Scientific Research from Japan Society for the Promotion of Science (B19300164) (H.S.), and Young Researchers Empowerment Project of Shinshu University (T.S.) from the Ministry of Education, Culture, Sports, Science and Technology (MEXT), Japan. M.M. and O.G. acknowledge financial support by the European Marie-Curie Research and Training Network on Arrested Matter under Grant No. MRTN-CT-2003-504712. The rHSA, HES$_{130}$, and MFG used in this study were gifts respectively from Nipro Co., Fresenius Kabi A.G., and B. Braun.

References

(1) Torchilin, V. P. *Nat. ReV. Drug DiscoVery* **2005**, *4*, 145-160

(2) Izumi, Y.; Sakai, H.; Hamada, K.; Takeoka, S.; Yamahata, T.; Kato, R.; Nishide, H.; Tsuchida, E.; Kobayashi, K. *Crit. Care Med.* **1996**, *24*, 1869-1873.

(3) Sakai, H.; Takeoka, S.; Park, S. I.; Kose, T.; Nishide, H.; Izumi, Y.; Yoshizu, A.; Kobayashi, K.; Tsuchida, E. *Bioconjugate Chem.* **1997**, *8*, 23-30.

(4) Chang, T. M. *Artif. Organs* **2004**, *28*, 789-794.

(5) Djordjevich, L.; Miller, I. F. *Exp. Hematol.* **1980**, *8*, 584-592.

(6) Phillips, W. T.; Klipper, R. W.; Awasthi, V. D.; Rudolph, A. S.; Cliff, R.; Kwasiborski, V.; Goins, B. A. *J. Pharmacol. Exp. Ther.* **1999**, *288*, 665-670.

(7) Sakai, H.; Horinouchi, H.; Yamamoto, M.; Ikeda, E.; Takeoka, S.; Takaori, M.; Tsuchida, E.; Kobayashi, K. *Transfusion* **2006**, *46*, 339-347.

(8) Sakai, H.; Masada, Y.; Horinouchi, H.; Yamamoto, M.; Ikeda, E.; Takeoka, S.; Kobayashi, K.; Tsuchida, E. *Crit. Care Med.* **2004**, *32*, 539-545.

(9) Yamazaki, M.; Aeba, R.; Yozu, R.; Kobayashi, K. *Circulation* **2006**, *114*, I220-I225.

(10) Sakai, H..; Sou, K.; Horinouchi, H.; Kobayashi, K.; Tsuchida, E. *J. Intern. Med.* **2008**, *263*, 4-15.

(11) Liu X.; Miller, M. J.; Joshi, M. S.; Sadowaska-Krowicka, H.; Clark, D. A.; Lancaster, J. R. Jr. *J. Biol. Chem.* **1998**, *273*, 18709-19713.

(12) Vaughn, M. W.; Huang, K. T.; Kuo, L.; Liao, J. C. *J. Biol. Chem.* **2000**, *275*, 2342-2348.

(13) Sakai, H.; Sato, A.; Takeoka, S.; Tsuchida, E. *J. Biol. Chem.* **2008**, *283*, 1508-1517.

(14) Sakai, H.; Hara, H.; Yuasa, M.; Tsai, A.G.; Takeoka, S.; Tsuchida, E.; Intaglietta, M. *Am. J. Physiol. Heart Circ. Physiol.* **2000**, *279*, H908-H915.

(15) Takeoka, S.; Ohgushi, T.; Terase, K.; Ohmori, T.; Tsuchida, E. *Langmuir* **1996**, *12*, 1755-1759.;

(16) Takeoka, S.; Terase, K.; Sakai, H.; Yokohama, H.; Nishide, H.; Tsuchida, E. *J. Macromol. Sci., Pure Appl. Chem.* **1994**, *A31*, 97-108.

(17) Glatter, O.; Kratky, O. *Small-Angle X-ray Scattering;* Academic: London, **1982**.

(18) Lindner, P.; Zemb, Th. Eds.; *Neutron, X-Ray and Light Scattering;* North-Holland: Amsterdam, **1991**.

(19) Peters, T. All About Albumin: Biochemistry, Genetics, and Medical Applications (Academic, New York, 1996).

(20) Meyuhas, D.; Nir, S.; Lichtenberg, D. *Biophys. J.* **1996**, *71*, 2602-2612.

(21) Sunamoto, J.; Iwamoto, K.; Kondo, H. *Biochem. Biophys. Res. Commun.* **1980**, *94*, 1367-1373.

(22) Otsubo, Y. *Langmuir* **1990**, *6*, 114-118.

(23) Tilcock, C. P.; Fisher, D. *Biochim. Biophys. Acta* **1982**, *688*, 645-652.

(24) Neu, B.; Meiselman, H. J. *Biophys. J.* **2002**, *83*, 2482-2490.

(25) Goto, Y.; Sakakura, S.; Hatta, M.; Sugiura, Y.; Kato, T. *Acta Anaesthesiol. Scand.* **1985**, *29*, 217-223.

(26) Asakura, S.; Oosawa, F. *J. Chem. Phys.* **1954**, *22*, 1255-1256.

(27) Asakura, S.; Oosawa, F. *J. Polym. Sci.* **1958**, *33*, 183-193.

(28) Vrij, A. *Pure Appl. Chem.* **1976**, *48*, 471-483.

(29) Bergenholtz, J.; Poon, W. C. K.; Fuchs, M. *Langmuir* **2003**, *19*, 4493-4503.

(30) Lekkerkerker, H. N. W.; Poon, W. C. K.; Pusey, P. N.; Stroobants, A.; Warren, P.B. *Europhys. Lett.* **1992**, *20*, 559-564.

(31) Ilett, S.M.; Orrock, A.; Poon, W. C. K.; Pusey, P. N. *Phys.Rev. E* **1995**, *51*, 1344-1352.

(32) Sakai, H.; Sato, A.; Takeoka, S.; Tsuchida, E. *Langmuir* **2007**, *23*, 8121-8128.

(33) Contaldo, C.; Plock, J.; Sakai, H.; Takeoka, S.; Tsuchida, E.; Leunig, M.; Banic, A; Erni, D. *Crit. Care Med.* **2005**, *33*, 806-812.

(34) Tsai, A. G.; Acero, C.; Nance, P. R.; Cabrales, P.; Frangos, J. A.; Buerk, D. G.; Intaglietta, M. *Am. J. Physiol. Heart Circ. Physiol.* **2005**, *288*, H1730-H1739.

(35) Tsai, A. G.; Intaglietta, M. *Biorheology* **2001**, *38*, 229-237.

(36) de Wit, C.; Schafer, C.; von Bismarck, P.; Bolz, S. S.; Pohl, U. *PflugersArch.* **1997**, *434*, 354-361.

(37) Kobayashi, K. *Biologicals* **2006**, *34*, 55-59.

(38) Sakai, H.; Tsai, A. G.; Kerger, H.; Park, S. I.; Takeoka, S.; Nishide, H.; Tsuchida, E.; Intaglietta, M. *J. Biomed. Mater. Res.* **1998**, *40*, 66-78.

(39) Webb, A. R.; Nash, G. B.; Dormandy, J. A.; Bennett, E. D. *Clin. Hemorheol.* **1990**, *10*, 287-296.

(40) Webb, A. R.; Barclay, S. A.; Bennett, E. D. *IntensiVe Care Med.* **1989**, *15*, 116-120.

(41) Traylor, R. J.; Pearl, R. G. *Anesth. Analg.* **1996**, *83*, 209-212.

(42) Medebach, M.; Moitzi, C.; Freiberger, N.; Glatter, O. *J. Colloid int. Sci.* **2007**, *305*, 88-93.

(43) Medebach, M.; Freiberger, N.; Glatter, O. *Rev. Sci. Instrum.* **2008**, *79*, 073907 (1-12).

(44) Pham, K. N.; Egelhaaf, S. U.; Pusey, P. N.; Poon, W. C. K.; *Phys. Rev. E* **2004**, *69*, 011503-1-13.

(45) Pham, K. N.; Egelhaaf, S. U.; Moussaïd, A.; Pusey, P. N. *Rev. Sci. Instrum.* **2004**, *75*, 2419-2431.

(46) Sou, K.; Naito, Y.; Endo, T.; Takeoka, S.; Tsuchida, E. *Biotechnol. Prog.* **2003**, *19*, 1547-1552.

(47) Sakai, H.; Masada, Y.; Takeoka, S.; Tsuchida, E. *J. Biochem. (Tokyo)* **2002**, *131*, 611-617.

(48) Sakai, H.; Tomiyama, K.; Sou, K.; Takeoka, S.; Tsuchida, E. *Bioconjugate Chem.* **2000**, *11*, 425-432.

(49) Orthaber, D., Bergmann, A. and Glatter, O. *J. Appl. Crystallogr.* **2000**, *33*, 218-225.

(50) Schnablegger, H.; Glatter, O. *Appl. Opt.* **1995**, *34*, 3489-3501.

(51) Lehner, D.; Kellner, G.; Schnablegger, H.; Glatter, O. *J. Colloid Int. Sci.* **1998**, *201*, 34-47.

(52) Weyerich, B.; Brunner-Popela, J.; Glatter, O. *J. Appl. Crystallogr.* **1999**, *32*, 197-209.

(53) Fritz, G.; Bergmann, A.; Glatter, O.; *J. Chem. Phys.* **2000**, *113*, 9733-9740.

(54) Fritz, G.; Glatter, O. *J. Phys.: Condens. Matter* **2006**, *18*, S2403-S2419.

(55) Koppel, D. E. *J. Chem. Phys.* **1972**, *57*, 4814-4820.

(56) Schnablegger, H.; Glatter, O. *Appl. Opt.* **1991**, *30*, 4889-4896.

(57) Frühwirth, T.; Fritz, G.; Freiberger, N.; Glatter, O. *J. Appl. Cryst.* **2004**, *37*, 703-710

(58) Glatter, O. *J. Appl. Cryst.* **1980**, *13*, 577-584.

(59) Glatter, O. *J. Appl. Cryst.* **1977**, *10*, 415-421.

(60) Sou, K.; Endo, T.; Takeoka, S.; Tsuchida, E. *Bioconjugate Chem.* **2000**, *11*, 372-379.

(61) Sato, T.; Sakai, H.; Sou, K.; Buchner, R.; Tsuchida, E. *J. Phys. Chem. B* **2007**, *111*, 1393-1401.

(62) Glatter, O. *J. Appl. Cryst.* **1981**, *14*, 101-108.

(63) Glatter, O. *Prog. Colloid Polym. Sci.* **1991**, *84*, 46-54.

(64) Mittelbach, R.; Glatter, O. *J. Appl. Cryst.* **1998**, *31*, 600-608.

(65) Rodriguez, C.; Naito, N.; Kunieda, H. *Colloid Surf. A* **2001**, *237*-246, 181.

(66) Sato, T.; Komatsu, T.; Nakagawa, A.; Tsuchida.E. *Phys. Rev. Lett.* **2007**, *98*, 208101 (1-4).

(67) Stradner, A.; Sedgwick, H.; Cardinaux, F.; Poon, W. C. K.; Egelhaaf, S. U.; Schurtenberger, P. *Nature* **2004**, *432*, 492-495.

(68) Liu, Y.; Chen, Fratini, E.; Baglioni, P.; W. R.; Chen, S. H. *Phys. Rev. Lett.*, **2005**, *95*, 118102 (1-4).

(69) Stradner, A.; Thurston, G. M.; Schurtenberger, P. *J. Phys.: Condens. Matter* **2005**, *17*, S2805–S2816.

(70) Chihara, J.; *Prog. Theor. Phys.* **1973**, *50*, 409-423.

(71) Madden W. G.; Rice, S. A. *J. Chem. Phys.* **1980**, *72*, 4208-4215.

人工臓器　移植医療の代替技術へ

テルモ　補助人工心臓「デュラハート」

普及へのロードマップ

欧州では20例の臨床試験が完了し、現在、承認申請中。2006年夏以降にも欧州で販売予定。米国では、06年度内での臨床試験申請を目指す。日本国内は、まだ臨床試験の計画を明らかにしていないが、海外の状況次第で数年以内にも臨床試験開始が期待できそう

ここが凄い

最新式の補助人工心臓。磁気浮上型遠心ポンプと独自設計により、従来機に比べ、小型でパワフル、耐久性があるのが特徴。従来の人工心臓の最大の課題である血栓もできにくい。当面は心臓移植までの暫定的使用が目的だが、将来的には、移植に代わる永久使用を目標とする

テルモ製は第3世代に相当。ケーブルが細くしなやかで、感染も少ないという

人工血液　異例の長期保存可能に

テルモ／オキシジェニックス

期限切れの血液からヘモグロビン（酸素運搬体）を抽出し、リポソーム（脂質）で包む（図はテルモ製）

人工赤血球

ここが凄い

本物の血液に比べ、血液型を問わず、6ヵ月以上の長期保存が可能で、緊急用に期待。本物の赤血球よりも小さく、酸素運搬力が強いので、脳梗塞などの治療にも応用

普及へのロードマップ

テルモは2007年3月にも日本と欧州で臨床試験を開始。オキシジェニックスも07年に臨床試験開始の予定で、適応症により承認までの期間は5〜7年を予測

再生医療　培養細胞で人体組織を再生

普及へのロードマップ

ジャパン・ティッシュ・エンジニアリングは、培養表皮の臨床試験を終了して、2004年10月に承認申請中。培養軟骨も臨床試験中で、近く承認申請する。いずれも今後2〜3年中に事業化見通し。テルモも心筋の再生で年度内にも臨床試験を開始。10年に事業化目指す

ここが凄い

生きた細胞で、心臓や肝臓、膵臓などの臓器を作る研究も進められているが、いまだ基礎研究段階。皮膚や軟骨などでは、実用段階入り。米国では、数千もの治療例があり、切手大の皮膚から約3週間で全身を覆うほどの技術が確立されている

ジャパン・ティッシュ・エンジニアリング／テルモなど

ジャパン・ティッシュ・エンジニアリング提供

ジャパン・ティッシュ・エンジニアリングの培養表皮は、患者自らの細胞を培養してシート状に作成し、重症火傷の治療などに用いる

が、より細く、小型化したファイバースコープとなり、画像技術も高精度化した。現在、ポリープなどでは小型の器具を取り付けた内視鏡での手術が開腹手術に代わって普及している。

最近では、オリンパスが薬のように飲み込むだけのカプセル型内視鏡を開発し、患者にとっても苦痛が少ないものに進化している。

将来的には、自走機能を持たせて、消化管内部の特定部位で薬剤を放出したり、病変組織を切除するといった「小型治療ロボット」化も視野に進展する。

人体に入った超小型潜水艇が治療を行なうというSF映画「ミクロの決死圏」のワンシーンを彷彿させる技術が現実化しつつある。

病気やケガで機能を失った身体器官を補う技術も進歩した。

その究極の例が臓器移植だろう。もっとも、臓器提供者の不足が課題で、先進の米国でも年間約二〇〇〇例、移植待機患者全体の数十分の一しか受けられない。

そこで、実用化待ちの人工臓器のほか、生きた細胞を用いて人為的に臓器・組織を再生する再生医療の研究が進められている。

心臓というポンプを人工的に作るのは一見簡単そうだが、[illegible]ことで発生する血

週刊ダイヤモンド 特大号
http://dw.diamond.ne.jp/
2006 4/8 特別定価570円

JAL-JAS統合は間違いだった! 日航再生の条件

5年以内に花開く 凄い技術 夢の製品

暮らしが変わる
富士写真フイルム「暗闇でも撮れるデジカメ」
住友電工「コンセントでどこでも高速ネット通信」
アデランス「細胞移植で頭髪が生える!?」

仕事が変わる
日立製作所「輸送力2.5倍のエレベーター」
セイコーエプソン「あらゆる電子機器を曲げる技術」

高まる安心
「危険を自ら察知する"走るコンピュータ"」
オリンパス「苦痛なしで飲み込めるカプセル型内視鏡」

持続可能な社会へ
ホンダ「ガソリン車並みに走行可能な燃料電池車」
「昆虫フェロモンで害虫撲滅」

春の大型特集 第2弾

新入社員と読みたい社訓

4.17 日経産業

人工赤血球

京都に製造設備

オキシジェニクス

パイオベンチャーのオキシジェニクス（東京・港、大村孝男社長）は、赤血球の代わりに酸素を運ぶ「人工赤血球」の製造設備を同社京都研究所（京都市）内に新設した。医薬品の製造品質管理基準（GMP）に準拠した設備。五月から稼働させて治験（臨床試験）用の製剤を作り、動物実験で安全性などを最終確認して二〇〇七年春にも日欧で治験を始める。

人工赤血球は酸素の運び役であるヘモグロビンを「リポソーム」と呼ぶ脂質のカプセルで包んで作る製剤。二年程度の長期保存が可能で、血液型を問わず輸血の代わりに利用できる。主に災害など緊急時の代替血液として有効とみられている。

新設した設備の製造能力は月産十一リットル。製造した人工赤血球は当面、「前臨床試験」と呼ぶ治験を前提とした動物実験に使い、安全性や効果の検証に役立てる。

〇七年春にも開始する治験で使う人工赤血球はすべて同施設で製造する。治験が順調に進み、対象となる患者が大幅に増える「第二相後期」に達した段階で、ニプロに製造委託する。それ以降、同施設は研究開発用の新製剤製造に転用する。

掲載日 2006年04月17日 日経産業新聞 017ページ

(C) 日本経済新聞社 無断複製転載を禁じます。

ニプロ、人工血液事業参入

バイオVBと業務提携

ニプロは人工血液事業に乗り出す。人工血液を託する。臨床試験（治験）を二〇〇八年から製造。臨床試験の進ちょく状況に応じ、段階的に量産化を進める。

人工血液は直径二百ナノ（ナノは十億分の一）㍍の微小カプセルに、約三週間の使用期限が切れた輸血用の血液から採取した有効成分を封入したもの。欧米で臨床試験が進んでいるが、まだ製品化には至っていない。二年程度の長期保存が可能で、血液型も問わないため、災害などの緊急備蓄用に全国で需要が見込めるという。

オキシジェニクスは人工血液を自社で製造し、来年春から日欧で臨床試験を始める。有効性の確認が順調に進み、対象患者が大幅に増える後期の臨床試験に着手するタイミングで、ニプロの製造に切り替える。一五年の製品化を目指す。

掲載日 2006年05月22日 日本経済新聞朝刊 000ページ

(C) 日本経済新聞社 無断複製転載を禁じます。

5.24 日経産業新聞

人工血液事業化
ニプロと提携
オキシジェニクス

バイオベンチャーのオキシジェニクス（東京・港、大村孝男社長）とニプロは二十三日、人工血液の事業化を目指して業務提携すると発表した。オキシジェニクスは二〇〇七年春から人工血液を自社製造して日欧で治験（臨床試験）を開始。安全性などの確認が進んで対象患者が増えるとみられる二〇〇八年からニプロに製造を委託する計画。

この人工血液は「人工酸素運搬体」と呼び、赤血球の代わりに酸素を運ぶ。約三週間の使用期限が切れた輸血用血液から有効成分を抽出し、直径二百五十ナノ（ナノは十億分の一）メートルの脂質の微小カプセルに包んで作る。

約二年の長期保存が可能。血液型も問わない。災害などの緊急備蓄の需要が見込まれている。

欧米メーカーが先行して治験を進めているが、製品化には至っていない。国内ではテルモが〇七年春に治験を始める計画を発表している。

掲載日 2006年05月24日 日経産業新聞 013ページ

(C) 日本経済新聞社 無断複製転載を禁じます。

〈日本ケミファ〉

電子公告など定款変更を提案へ

日本ケミファは22日の取締役会で、電子公告ができるようにするためなどの定款変更議案を、6月29日開催予定の第74回定時株主総会に付議することを決めた。公告閲覧の利便性向上や株主総会事務処理の効率化などが主な目的。また取締役会の機動的、効率的運営を図るため、取締役全員の同意があり、監査役が異議を述べないときに限り、取締役会の書面決議を可能とする内容も盛り込まれている。

〈アボットなど3社〉

「ホクナリンテープ」表面に品名表示

アボット ジャパン、マルホ、日東電工は22日、貼付型の気管支拡張剤「ホクナリンテープ」（一般名＝ツロブテロール）の表面に、安全確保を目的として、製品名を表記したと発表した。テープ表面に製品名表示がないと、患者、医療従事者などが、何の薬剤を貼り付けたのか分からないという問題点が指摘されていた。今回、テープ表面に製品名を表示することで、その問題に対応した。

☆〈オキシジェニクス〉

酸素運搬体製造でニプロと提携

バイオベンチャーのオキシジェニクスは23日、ニプロと人工酸素運搬体「オキシジェンキャリア（OXY－0301）」の製造で業務提携した。両社は2004年に3年間の共同開発契約を結んだが、今回の製造契約締結で、ニプロは07年からOXY－0301のGMP（医薬品の製造管理および品質管理に関する基準）準拠製造プラントの設計を開始し、08年から同治験薬の製造、早期の大量製造と実用化を目指す。

〔人　事〕

◇日本ケミファ（6月29日付予定）【役員異動】〔新任取締役候補〕社外取締役（非常勤）・茂腹敏明（新任監査役）社外監査役（非常勤）・高橋剛（退任予定監査役）山中徹監査役（非常勤）

◇アクロネット（5月23日付）【役員人事】

代表取締役社長・植松尚

〔開　催〕日本能率協会は6月26日（月）午前10時、大阪市北区の同協会関西地域事業部研修室で、「第11回医薬品GMP教育訓練担当者養成コース」を開催する。ファーマサービスイコマ代表の稲津邦平氏が、①GMP教育訓練にかかわる法規条項などの概要②GMPの歴史とSOPの情報③情報の効果的活用――などについて講演する。参加費は同協会会員3万6750円、非会員4万2000円で、5月31日（水）までの申し込みは、それぞれ3万1500円、3万7800円の割引価格（いずれも税込み）。問い合わせ・申し込みは、同協会関西地域事業部（TEL 06－4797－2052、FAX 06－4797－2051）へ。

〈本号9頁〉

●わかもと製薬　2006年3月期決算概況

【連結】　単位：百万円、％

	売上高	営業利益	経常利益	当期利益
当　期	10,185（1.5）	673（△8.6）	744（△12.3）	448（△8.0）
次期中間期予想	5,000	—	320	200
次期通期予想	10,200	—	670	420

【単体】

	売上高	営業利益	経常利益	当期利益
当　期	10,142（1.5）	650（△10.0）	731（△13.6）	441（△9.1）
次期中間期予想	4,980	—	310	195
次期通期予想	10,150	—	655	410

配当実績	中間　2.50円	期末　2.50円	年間　5.00円
次期配当予想	中間　2.50円	期末　2.50円	年間　5.00円

輸血不足を解決するか
人工"酸素"運搬体（人工赤血球）
テルモなど日欧米で研究開発進む

オキシジェニクスの「Oxgen Carrier」の構造と特徴

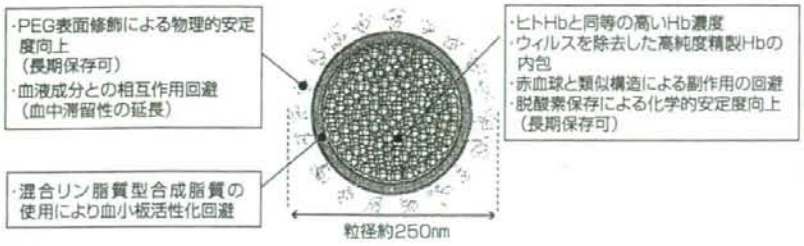

人工酸素運搬体が人工血液の可能性を拡げようとしている。

我々ヒトという生物は、全身に約60兆個と言われる細胞と、それを中枢制御する脳というスーパーコンピューターから成り立っている。全身の臓器、組織など全ての生命活動の維持には膨大なエネルギーを必要とし、そのエネルギーは基本的には、細胞内で糖などの呼吸基質と酸素との酸化反応で生み出されている。細胞呼吸と呼ばれる代謝である。

体内に取り込まれた、エネルギーを作り出す元となる酸素を運搬する細胞は血液全体の45％の量である赤血球であり、酸素が結合するのは赤血球にあるヘモグロビンというタンパク質のヘムという真っ赤な分子の真ん中にある鉄分である。各臓器で、酸素はこの鉄から離れ、細胞に存在する間、解糖系、クエン酸回路を経てミトコンドリアの電子伝達系に取り込まれてエネルギー産生に使われるのだ。それだけに手術などの治療に用いられる血液はまさに余命の源となる。

ところが世界的に見て、輸血用の血液は、「ＡＩＤＳ」等の問題もあって供給不足の状況にあるとされる。

厚生労働省の資料によれば、日本において、日本赤十字社が製造・供給している輸血用血液製剤はすべて国内の献血で賄われており、その年間確保量は約２００万ℓ。その内の約半分が赤血球製剤という。輸血用製剤の有効期限は全血製剤と赤血球製剤で21日間（3週間）、血小板製剤が採血後72時間とされている。この赤血球製剤の使用期限の限界があることから、現行の献血システムで救急救命用途や災害用備蓄として賄いきれていないという現状がある。

"日本発"の世界的人工血液技術

そこで開発が進められているのが、酸素を運搬するという、生命にとって重要な機能を備えた「人工血液」＝「人工赤血球」である。欧米の数

社のベンチャー企業、日本ではテルモ、そしてバイオベンチャーのオキシジェニクスが研究・開発に携わっている。

ヒトや牛のヘモグロビンを使って造られて来たこれまでの「人工血液」は、「ヘモグロビンのガス交換（酸素⇄二酸化炭素）が実際の赤血球とは異なる」、「ヘモグロビンそのものは、その大きさ、形状から血管壁の開窓を通過してしまい、NO（一酸化窒素）やCOと結合してしまう」など実用段階での安全性が確認されないことから、実用化されていないのが現状らしい。

そこで日本のオキシジェニクス、テルモの世界的に見て、2社のみが開発したのが、酸素運搬体であるヘモグロビンをリポソームという脂質の二重膜で内包する技術である。テルモとオキシジェニクスとではその技術に違いがあるらしい。人工酸素運搬体の特長といえば、例えばオキシジェニクスの「Oxygen Carrier」の場合、室温での長期保存安定性があるとされ、粒経250㎚に設計されていることから10～100㎚とされる血管壁の開窓を通過しない。特に、他社海外製品の修飾型ヘモグロビンと比較してNOやCOとの相互作用を引き起こさない適切なサイズ（250㎚）に設計されているものであるという。さらに250㎚という粒経は8000㎚のヒト赤血球と比較した場合、狭窄血管への酸素輸送が可能で、ガン、虚血性疾患治療に使われる「酸素治療薬」としての使用の可能性も高いという。

医薬品業界ではDDS（ドラッグデリバリーシステム）、またGDS（ジーンデリバリーシステム）といわれるのが一般的だが、「G＝GAS」で、ガスデリバリーシステムという概念もあり、酸素を代表とする、生体内に存在する各種ガスの働きを追求し、ガスバイオロジーをベースとした創薬研究にも取り組む動きがここに来て出て来たと言えるだろう。特に、治療薬として酸素が活用されるのは注目すべきテーマだ。尚、同社はGMP製造設備を整えた京都研究所で製造された製剤を用いて来年には臨床試験（治験）を開始する計画である。

身体におけるガスの働きを創薬に応用する

慶應義塾大学医学部 医化学教室 末松誠教授

前述のオキシジェニクス（本社・東京都港区）は早稲田大学理工学部と慶應義塾大学医学部の共同研究による技術シーズの事業化を目的に、02年12月に設立されたベンチャー企業である。本社の他、京都と横浜に研究所を持ち、慶應義塾大学医学部信濃町キャンパス（東京都新宿区）総合医科学研究棟に基礎研究センターを置く。人工酸素運搬体（酸素治療薬）「Oxygen Carrier」の研究開発、用途開発事業を中心に、体内におけるGasの働き＝「Gas Biology」をベースとした創薬開発事業も進めている。この「Gas Biology」を研究テーマとして数年前から取り組んで来たのが、同社の設立にも関わり、現在、技術顧問となっている慶應義塾大学医学部医化学教室の末松誠教授である。

末松教授の研究テーマである「Gas Biology」の「Gas」とは主に酸素、そしてNO（一酸化窒素）とCO（一酸化炭素）のことを指す。まず、NOに関して研究開発したものについては、「ヘモグロビンは1分子当たりα-1、α-2、β-1、β-2の4つのポケットがあり、2つのαのポケットをNOで満たした（NOで安定させた）α-NOを持ったヘモグロビンは酸素乖離能が高く（酸素の放出量が多く）なり、解糖系の代謝が活発になる。また血管拡張作用を持つATP（アデノシンシリン酸）の放出を活発にし、血流を流れやすくする。ヘモグロビンは局所の酸素濃度を感知しながら各種の代謝物を活発に出し入れするメタボリックスイッチとして作用することが明らかになっているわけで、虚血性疾患、肝障害など、低酸素状態になっているところにおけるNOを処理（付加）した赤血球の効果がラットを使った実験により確認できている」（末松教授）と説明する。またCOについては、輸血して保存されている血液は4℃でも代謝が起きているがCOを付加することで代謝が抑えられることを確認しており、輸血液の保存に役立つという。

研究開発に使うNOは溶剤を使い、直接ガスのNOを使うものではないが、COはガスディーラーから購入したものを使っているそうだ。

命を守る最前線で。
健やかな暮らしを願う
心の中に。
いつも星医療酸器は
あなたといたい。

30年以上にわたる医療用ガスの提供サービス。その中で私たちは、常に「命」と「暮らし」に真正面から向き合い、自らの可能性を切り拓いてきました。そして今、高齢化・情報化が進む社会に即応するべく、新しい事業の開拓・確立へ。社会との接点は、ますます広がりつつあります。

株式会社 星医療酸器
〒121-0836 東京都足立区入谷7-11-12
TEL 03-3899-8855 FAX 03-3899-5661
URL http://ns1.hosi.co.jp/

人工赤血球
実用化に向けて最終段階

「人工赤血球」が体の全細胞の呼吸に必要な充分量の酸素を運搬する

日本の献血・輸血システムは世界的水準にあり、国民の医療と健康福祉に多大の貢献をしている。献血血液の厳重な検査により、安全性のさらなる向上が図られている。他方、「人工赤血球」の開発が厚生労働省の積極的な支援も受けて急速に進められている。その特徴は、1血液型がないのでただちに投与可能2ウィルスなど感染源がない3室温で2年間安定なので災害用に備蓄して救急救命に使用できる4大量投与しても体内の代謝系を経て分解排泄される、などである。また、5原料確保のため遺伝子組換え技術によるヘモグロビン、アルブミンの供給技術も利用可能になってきている。思いきった国策の採用とあわせ、国民の健康福祉と安全の確保に資くべき貢献をもたらすことになろう。

実現が最も近いとされる人工赤血球が、土田英俊早稲田大学教授らの開発した「ヘモグロビン小胞体」だ。酸素結合タンパク質「ヒトヘモグロビン」約3万個を脂質二分子膜で包んだ直径250 nmの小球粒子で、ヘモグロビン分子単体の毒性をさえぎっている。小林紘一慶應義塾大学医学部教授ほか、国内外の研究機関との共同で、動物投与試験による安全度と効能の確認を進めている。大量出血によるショック状態にヘモグロビン小胞体を投与すると、酸素供給が速やかに回復し救命できること、微小なヘモグロビン小胞体は血管中に均一に分散し、赤血球の到達が困難な末梢組織まで酸素供給できることがわかった。霊長類での安全性も確認済みで、2006年内に臨床試験を申請する予定だ。

Newton スーパーテクノロジー・ビジュアル報告、明日を一新する「値千金」の技術３２
(株)ニュートンプレス 2006. 5.

'06.6.11

アラヌー

オキシジェニクスがニプロと

人工酸素運搬体の製造で契約

バイオベンチャーのオキシジェニクス（東京都港区）は5月23日、ニプロとの間で、赤血球の代用品となる人工酸素運搬体「Oxygen Carrier（開発コード＝OXY－0301）」の将来製造に関する業務契約を締結したと発表した。

同社は、ニプロと2004年から3年間の共同開発契約を結び、製造技術開発に着手。5月にミニスケールの治験薬製造プラントを稼働させ、ニプロが量産化に向けたスケールアップの検討を進めることとなった。

今回の契約によりニプロは、08年からOXY－0301の治験薬の製造を開始する。両社は、研究・開発に関する情報交換などをさらに強化し、今後、海外戦略についても検討していく。

同社は、早稲田大理工学部と慶応大医学部の共同研究による技術シーズを事業化するため、02年12月に設立された。